Eur. Phys. J. E **21**, 199–207 (2006)
DOI 10.1140/epje/i2006-10060-x

THE EUROPEAN PHYSICAL JOURNAL E

Effect of large degrees of polydispersity on strongly segregated block copolymers

M.W. Matsen[a]

Department of Mathematics, University of Reading, Whiteknights, Reading RG6 6AF, UK

Received 5 November 2006
Published online: 13 December 2006 –

Abstract. We investigate the effect of polydispersity on the lamellar phase of a diblock copolymer melt using self-consistent field theory (SCFT). A previous SCFT calculation predicted that polydispersity increases the domain spacing consistent with experiment, but it also suggested that the effect vanishes with increasing segregation contrary to experiment. We attribute this disagreement to a problem of slow convergence of the Gaussian-quadrature technique used to integrate over the molecular-weight distribution when either the segregation or polydispersity index is large. Here the problem is overcome by a new efficient algorithm that allows high-order quadratures for relatively little computational cost. When implemented, we find that the elevated domain spacing does indeed persist into the strong-segregation regime consistent with experiment. This conclusion is also substantiated by the analytical strong-segregation theory (SST).

PACS. 82.35.Jk Copolymers, phase transitions, structure – 61.46.-w Nanoscale materials

1 Introduction

The study of block copolymer melts has received considerable attention over the past couple decades, and has reached a point where there is good quantitative agreement between experiment and theory [1]. The model system upon which most of this research has focused is that of the monodisperse AB diblock architecture, where the behavior is governed by just two parameters: the composition of the diblock, $f \equiv N_A/N$, and the degree of segregation, χN. Here χ is the usual Flory-Huggins A-B segment interaction parameter and $N \equiv N_A + N_B$ is the total number of A and B segments composing each molecule. Although researchers have explored more complicated architectures, numerous kinds of blends, solutions, and exotic polymer types, there has been a distinct aversion to polydisperse systems. Polydispersity is seen as an undesirable feature that simply complicates quantitative studies, both theoretically and experimentally. There is also a concern that the tendency to self-assemble into well-ordered periodic morphologies might be compromised by too much polydispersity [2]. Furthermore, as the constituent molecules become distinguishable, the undesirable effect of macrophase separation becomes an increasing possibility [3].

Although there are good reasons for avoiding the complication of polydispersity, the anionic polymerization technique used to produce near monodisperse molecules is generally expensive and naturally this impedes the commercialization of block copolymer materials. Fortunately, new mechanisms of controlled radical polymerization are now offering more economical ways of synthesising block copolymers, but they generally result in large degrees of polydispersity [2,3]. This has proven to be the necessary impetus to initiate new research towards the understanding of how polydispersity modifies the known behavior of monodisperse systems and determining whether or not the desirable features of block copolymer materials survive. In reality, there is the distinct possibility that polydispersity will result in new advantageous properties.

The first systematic experiment to examine polydispersity effects in block copolymer melts was conducted only a few years ago in 2003 by Matsushita *et al.* [4]. They examined discrete distributions formed by mixing nine relatively monodisperse samples, all of similar total molecular weight, N, but with different compositions spanning the full range of f. The blends were all chosen with an overall symmetric composition, and, as a result, most formed lamellar microstructures. They found that the polydispersity increased the lamellar period, and at sufficiently high polydispersity, macrophase separation occurred producing coexistence between a well-ordered lamellar microstructure and some poorly ordered morphology.

More recently, Lynd and Hillmyer [5] have conducted a model experiment on a different system, where one block (*e.g.*, B) is monodisperse while the other block (*e.g.*, A) is polydisperse with a distribution $p(\sigma)$. (Here

[a] e-mail: m.w.matsen@reading.ac.uk

$p(\sigma)\mathrm{d}\sigma$ represents the fraction of diblock molecules for which the A-block polymerization lies between $fN\sigma$ and $fN(\sigma + \mathrm{d}\sigma)$.) Their study produced two main conclusions. First, polydispersity in the A block causes the phase boundaries to shift towards larger f. This result had already been suggested by some preliminary calculations [6], and has now been collaborated by more thorough calculations [7] and by further experiments [3]. Second, they found that polydispersity causes a significant increase in the domain spacing, much like that observed for the system studied by Matsushita *et al.* Again the qualitative trend was anticipated by weak-segregation calculations [8], but Lynd and Hillmyer also performed their own quantitative calculations using a self-consistent field theory (SCFT) algorithm introduced by Sides and Fredrickson [6]. For weak to intermediate segregations, the SCFT predicted an increased domain spacing inline with their experiment, but it also suggested that the elevated spacing vanishes in the strong-segregation limit. This was in clear contradiction with the results of their experiment.

The SCFT calculation proceeds in the same way as for monodisperse melts [9], but with the substitutions

$$\phi_\alpha(\mathbf{r}) = \int_0^\infty \mathrm{d}\sigma p(\sigma)\phi_\alpha(\mathbf{r};\sigma), \tag{1}$$

$$\ln \mathcal{Q} \to \int_0^\infty \mathrm{d}\sigma p(\sigma) \ln \mathcal{Q}(\sigma), \tag{2}$$

where $\phi_\alpha(\mathbf{r};\sigma)$ is the concentration of α-type segments and $\mathcal{Q}(\sigma)$ is the single-chain partition function for diblock copolymers with $fN\sigma$ A-type segments and $(1-f)N$ B-type segments. (N is now the number-averaged degree of polymerization for the entire diblock.) As for virtually all theoretical calculations, Sides and Fredrickson considered the Schulz-Zimm distribution [10],

$$p(\sigma) = \frac{k^k \sigma^{k-1} \exp(-k\sigma)}{\Gamma(k)}, \tag{3}$$

for which the polydisperse index of the A-block is $\mathrm{PDI}_A = (k+1)/k$. Although this extension to polydisperse diblocks is straightforward, there is the computational challenge of integrating over the semi-infinite range $\sigma = 0$ to ∞. Numerical integration approximates the continuous integral by a discrete sum, but the computational cost can become exorbitant if a large number of molecular weights, σ, needs to be sampled. Sides and Fredrickson circumvented this problem by utilizing a Gauss-Laguerre quadrature approximation,

$$\int_0^\infty \mathrm{d}\sigma p(\sigma) f(\sigma) \approx \sum_{g=1}^{n_g} p_g f(\sigma_g), \tag{4}$$

where the set of points $\{\sigma_g\}$ and the weights $\{p_g\}$ are chosen according to a well-prescribed procedure [11]. Naturally, the approximation improves as the order, n_g, of the quadrature is increased, but Sides and Fredrickson found that $n_g \leq 8$ was generally sufficient. It was essential that n_g not be too large, because the computational cost was roughly proportional to the number of evaluations of $\phi_\alpha(\mathbf{r};\sigma)$. Naturally, the concern is greatly exacerbated when both blocks are polydisperse, because in that case double integrals need to be performed.

Cooke and Shi [7] have since proposed an alternative approach that uses the approximation

$$p(\sigma) \approx \delta(\sigma - 1) + \frac{1}{2}(\mathrm{PDI}_A - 1)\delta''(\sigma - 1), \tag{5}$$

which assumes that the polydispersity index, PDI_A, is small. At this level of approximation, the detailed shape of the distribution does not enter, and thus their results are very general. Another advantage of their approach is its efficiency, allowing them to easily cope with diblock molecules where both blocks are polydisperse. In their study, they found that an asymmetry in the degrees of polydispersity causes a significant shift in the phase boundaries, qualitatively consistent with experiments [3, 5]. Furthermore, they reconfirmed the previous prediction that polydispersity causes an elevation in the domain spacing. However, they did not investigate strong segregations and the nature of their calculation prevented them from exploring the high polydispersities characteristic of the Lynd-Hillmyer experiment.

Our present study is motivated by the discrepancy [5] between experiment and theory in regards to the increased domain spacing in well-segregated melts. We find that the Gaussian-quadrature scheme converges slowly when the segregation or the degree of polydispersity is large, which presumably led to inaccurate SCFT predictions. Rectifying this requires an increase in n_g by one or two orders of magnitude, which greatly compromises the efficiency of the calculation. However, we are able to optimise the algorithm using a spectral approach, so much so that the computational cost of quadratures of order $n_g \sim 100$ is only a couple times that of a monodisperse melt.

2 Theory

Our new SCFT algorithm for polydispersity block copolymers follows our previous spectral method introduced in reference [9] for monodisperse melts. In this method, all functions of position, such as the self-consistent fields and the polymer concentrations, are expanded as

$$w_\alpha(\mathbf{r}) = \sum_i w_{\alpha,i} f_i(\mathbf{r}), \tag{6}$$

$$\phi_\alpha(\mathbf{r}) = \sum_i \phi_{\alpha,i} f_i(\mathbf{r}), \tag{7}$$

respectively, where $\alpha = A$ or B. The basis functions, $f_i(\mathbf{r})$, are chosen to be eigenfunctions of the Laplacian,

$$\nabla^2 f_i(\mathbf{r}) = -\frac{\lambda_i}{D^2} f_i(\mathbf{r}), \tag{8}$$

where D is the period of the morphology. The functions are naturally orthogonal and can be normalized such that

$$\frac{1}{\mathcal{V}} \int \mathrm{d}\mathbf{r} f_i(\mathbf{r}) f_j(\mathbf{r}) = \delta_{ij}, \tag{9}$$

where $\mathcal{V}$ is the volume of the melt. To improve computational efficiency, the basis functions are generally chosen so that they possess the symmetry of the phase under consideration, although this is not necessary.

Central to the spectral algorithm is the transfer matrix,

$$\mathbf{T}_A(s) \equiv \exp(\mathbf{A}s), \tag{10}$$

which involves the symmetric matrix, $\mathbf{A}$, defined by

$$A_{ij} = -\frac{a^2 N \lambda_i}{6D^2}\delta_{ij} - \sum_k w_{A,k}\Gamma_{ijk}, \tag{11}$$

where a is the statistical segment length and

$$\Gamma_{ijk} = \frac{1}{\mathcal{V}}\int \mathrm{d}\mathbf{r} f_i(\mathbf{r}) f_j(\mathbf{r}) f_k(\mathbf{r}). \tag{12}$$

The transfer matrix is evaluated by first writing

$$\mathbf{A} = \mathbf{V}_A \mathbf{D}_A \mathbf{V}_A^T, \tag{13}$$

where $\mathbf{D}_A$ is a diagonal matrix containing the eigenvalues, $d_{A,i}$, of $\mathbf{A}$ and the columns of $\mathbf{V}_A$ contain the normalized eigenvectors of $\mathbf{A}$. Once the eigenvalues and corresponding eigenvectors are determined, the components of the transfer matrix are given by

$$T_{A,ij}(s) = \sum_k V_{A,ik}\exp(d_{A,k}s)V_{A,jk}. \tag{14}$$

Likewise, there is a second transfer matrix, $\mathbf{T}_B(s) \equiv \exp(\mathbf{B}s)$, where $\mathbf{B}$ satisfies the same equation (11), but with the coefficients of $w_A(\mathbf{r})$ replaced with those of $w_B(\mathbf{r})$.

In terms of the two transfer matrices, the components of the overall A- and B-segment concentrations become

$$\phi_{A,i} = \int_0^\infty \mathrm{d}\sigma \frac{p(\sigma)\mathcal{V}}{\mathcal{Q}(\sigma)} \sum_{jk\ell} \Gamma_{ijk} T_{B,\ell 1}(1-f) \times \int_0^{f\sigma} \mathrm{d}s T_{A,j1}(s) T_{A,k\ell}(f\sigma - s), \tag{15}$$

$$\phi_{B,i} = \int_0^\infty \mathrm{d}\sigma \frac{p(\sigma)\mathcal{V}}{\mathcal{Q}(\sigma)} \sum_{jk\ell} \Gamma_{ijk} T_{A,\ell 1}(f\sigma) \times \int_0^{1-f} \mathrm{d}s T_{B,j\ell}(s) T_{B,k1}(1-f-s), \tag{16}$$

respectively, where

$$\mathcal{Q}(\sigma) = \mathcal{V}\sum_i T_{A,i1}(f\sigma) T_{B,i1}(1-f). \tag{17}$$

Using equation (14), these expressions can be rewritten as

$$\phi_{A,i} = \sum_{jk\ell mn} \Gamma_{ijk} V_{A,jm} V_{A,1m} V_{A,kn} V_{A,\ell n} \times T_{B,\ell 1}(1-f) J_{mn}, \tag{18}$$

$$\phi_{B,i} = \sum_{jk\ell mn} \Gamma_{ijk} V_{B,jm} V_{B,\ell m} V_{B,kn} V_{B,1n} \times K_\ell I_{B,mn}(1-f), \tag{19}$$

where

$$I_{\alpha,ij}(t) \equiv \int_0^t \mathrm{d}s \exp(d_{\alpha,i}s + d_{\alpha,j}(t-s)), = \begin{cases} \frac{\exp(td_{\alpha,i}) - \exp(td_{\alpha,j})}{d_{\alpha,i} - d_{\alpha,j}}, & \text{if } d_{\alpha,i} \neq d_{\alpha,j}, \\ t\exp(td_{\alpha,i}), & \text{if } d_{\alpha,i} = d_{\alpha,j}, \end{cases} \tag{20}$$

$$J_{ij} \equiv \int_0^\infty \mathrm{d}\sigma p(\sigma) \frac{I_{A,ij}(f\sigma)\mathcal{V}}{\mathcal{Q}(\sigma)}, \tag{21}$$

$$K_i \equiv \int_0^\infty \mathrm{d}\sigma p(\sigma) \frac{T_{A,i1}(f\sigma)\mathcal{V}}{\mathcal{Q}(\sigma)}. \tag{22}$$

In this way, the polydispersity only enters when evaluating J_{ij} and K_i, which is readily done using the Gaussian-quadrature scheme. The rest of the calculation remains exactly the same as for the monodisperse melt.

By isolating the integration over σ to the quantities J_{ij} and K_i, considerable computational time is saved relative to n_g independent calculations of $\phi_\alpha(z;\sigma)$. However, there is an even bigger time saving to be had by noting that for σ larger than some value σ^*, the transfer matrix in equation (14) becomes dominated by the terms involving the largest eigenvalue, which we label as $d_{A,1}$. In this limit,

$$\mathcal{Q}(\sigma) \approx \mathcal{Q}(\sigma^*)\exp(d_{A,1}f(\sigma - \sigma^*)) \tag{23}$$

becomes linear in σ, while the ratios,

$$\frac{I_{A,ij}(f\sigma)}{\mathcal{Q}(\sigma)} \approx \begin{cases} \frac{f\sigma^* \exp(f\sigma^* d_{A,1})}{\mathcal{Q}(\sigma^*)}, & \text{if } i=j=1, \\ \frac{\exp(f\sigma^* d_{A,1})}{(d_{A,1}-d_{A,j})\mathcal{Q}(\sigma^*)}, & \text{if } i=1, j\neq 1, \\ \frac{\exp(f\sigma^* d_{A,1})}{(d_{A,1}-d_{A,i})\mathcal{Q}(\sigma^*)}, & \text{if } i\neq 1, j=1, \\ 0, & \text{if } i,j\neq 1, \end{cases} \tag{24}$$

$$\frac{T_{A,i1}(f\sigma)}{\mathcal{Q}(\sigma)} \approx \frac{V_{A,i1}V_{A,11}\exp(f\sigma^* d_{A,1})}{\mathcal{Q}(\sigma^*)}, \tag{25}$$

in equations (21) and (22), respectively, become independent of σ. When the order, n_g, of the Gaussian quadrature is large, the vast majority of $\{\sigma_g\}$ are sufficiently large to take advantage of this *ground-state dominance* approximation [12], and thus the computational cost is tremendously reduced.

The one other place that the polydispersity distribution enters the SCFT calculation is in the evaluation of the free energy,

$$\frac{F}{nk_BT} = -\int_0^\infty \mathrm{d}\sigma p(\sigma)\ln\mathcal{Q}(\sigma) - \chi N\sum_i \phi_{A,i}\phi_{B,i}, \tag{26}$$

where n is the total number of molecules in the melt. We will need the free energy, F, in order to determine the equilibrium domain size, D, of the lamellar phase. Again the integral over σ can be approximated by the Gaussian quadrature, and, as before, the sum over $\sigma_g \geq \sigma^*$ becomes trivial with use of the ground-state dominance approximation in equation (23).

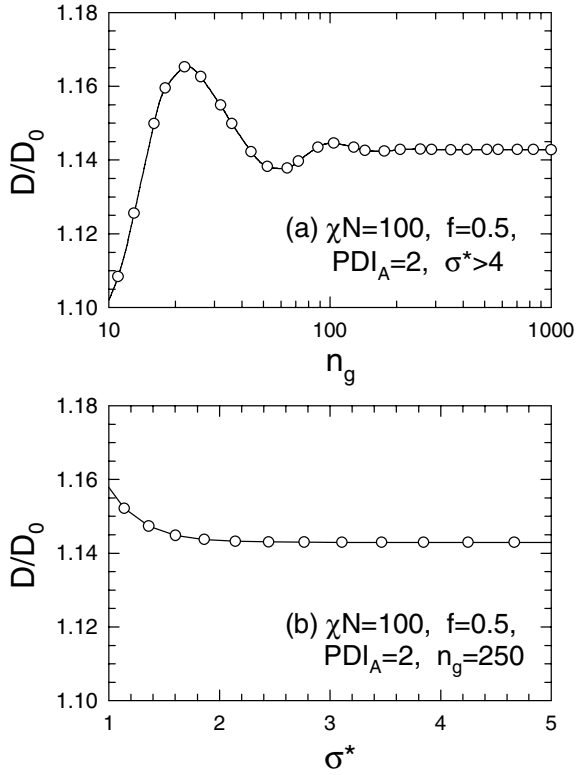

Fig. 1. (a) Convergence of the domain spacing, D, as the order, n_g, of the Gaussian-quadrature approximation (Eq. (4)) is increased. (b) Convergence as the molecular weight, σ^*, for the application of the ground-state dominance approximation (Eqs. (24) and (25)) is increased. In both cases, the reference spacing, D_0, is that of a monodisperse melt.

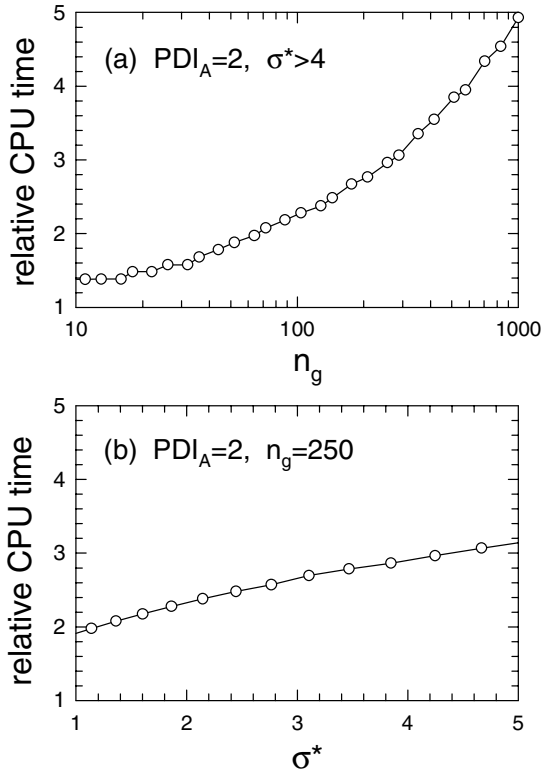

Fig. 2. Computational time for the calculations in Figure 1 relative to that of a monodisperse melt.

3 Results

In this paper, we focus on the lamellar morphology, but before doing so we investigate the convergence of the Gaussian quadrature (Eq. (4)). This is done in Figure 1 by examining the equilibrium domain spacing, D, relative to that of the monodisperse melt, $D_0 = 2.3367aN^{1/2}$, for a case of large segregation ($\chi N = 100$) and high polydispersity ($\mathrm{PDI}_A = 2$). The upper plot shows the convergence as the order, n_g, of the quadrature is increased, while the ground-state dominance is applied for all values of σ_g greater than 4. The lower plot illustrates the effect of varying the point, σ^*, at which the ground-state dominance is implemented. From this careful examination, we see that D/D_0 converges to 1.1428, which incidentally matches well with the SST prediction of $(3/2)^{1/3} = 1.1447$ derived in the appendix. (We will soon see that this is a fortuitous rather than characteristic level of agreement between SCFT and SST.) Similar examination reveals that the necessary value of n_g increases rapidly with χN; we will use $n_g = 50$, 125, 250 and 800 for $\chi N = 25$, 50, 100 and 400, respectively, which is sufficient that the numerical inaccuracy is undetectable on the scale of our plots. Of course, the necessary n_g reduces to 1 as $\mathrm{PDI}_A \to 1$; we find that sufficient accuracy is maintained if we allow n_g to decrease linearly with PDI_A. The necessary value of σ^* for good convergence is relatively insensitive to the parameters, and so all our calculations are done with σ^* equal to the first value of $\sigma_g > 4$.

To illustrate the computational efficiency of our algorithm, Figure 2 plots the CPU time used to generate the data points in Figure 1. The actual computational time depends strongly on the number of basis functions required by the expansions in equations (6) and (7), and so we compare the polydisperse calculations to that of a monodisperse calculation performed with the same number of basis functions. In this way, the relative times plotted in Figure 2 remain more or less valid for all block copolymer morphologies with a $\mathrm{PDI}_A = 2$. As illustrated in Figure 1, the order of the Gaussian quadrature must be $n_g \approx 250$ for accurate results when the segregation is $\chi N = 100$, but even this fairly extreme case only increases the CPU time by a factor of ~ 3 over that of the monodisperse calculation.

Now that the issue of convergence has been addressed, Figure 3 examines the equilibrium domain spacing of the lamellar phase over a wide range of conditions. For comparison, the predictions of the analytical strong-segregation theory (SST) described in the appendix are included with dashed curves. The upper plot shows the relative spacing, D/D_0, as a function of polydispersity, PDI_A, for a series of segregations, χN, at the fixed composition, $f = 0.5$. The SCFT results are far more linear than the SST curve, but the SCFT curves do begin to take on a similar shape by $\chi N = 400$. Certainly, there is

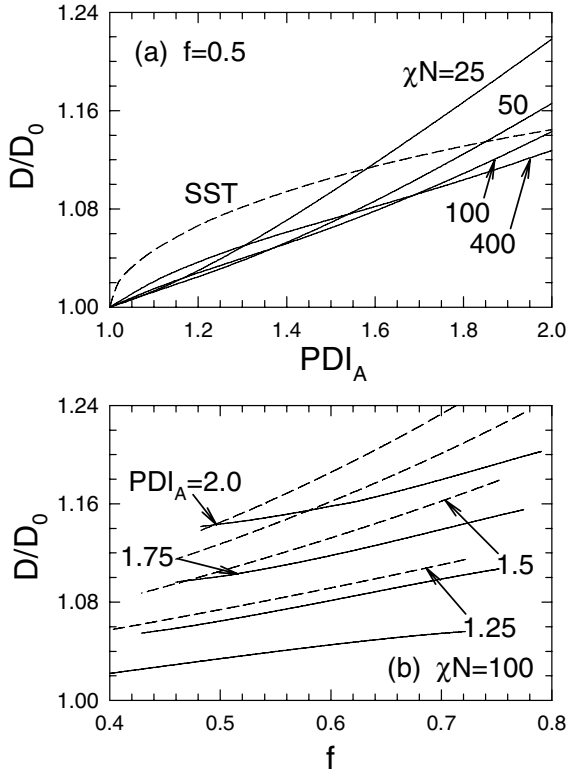

Fig. 3. (a) Domain spacing, D, relative to that of a monodisperse melt, D_0, plotted as a function of the A-block polydispersity, PDI_A. The solid curves are calculated with SCFT at various levels of segregation, and the dashed curve is calculated with SST. (b) Analogous plot but as a function of diblock composition, f, with a fixed segregation of $\chi N = 100$ and various levels of A-block polydispersity.

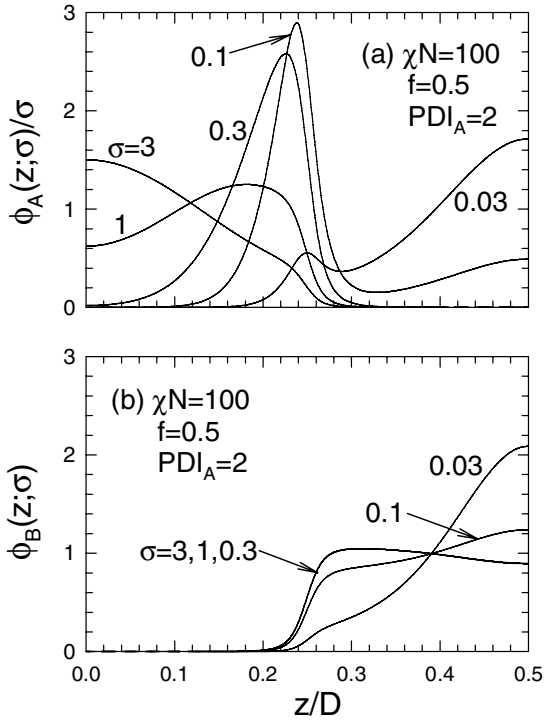

Fig. 4. (a) A-segment distribution, $\phi_A(z;\sigma)$, plotted for various A-block molecular weights, σ. (b) Analogous plot showing the B-segment distribution. In both cases, the horizontal scale extends from the middle of an A-rich domain ($z = 0$) to the middle of a B-rich domain ($z = D/2$).

every reason to believe that the SCFT results will asymptotically approach the SST curve in the limit of large χN, rather than approaching $D/D_0 = 1$ as suggested by reference [5]. Indeed, sizable inaccuracies in the earlier SCFT calculations are clearly evident. For $\mathrm{PDI}_A = 2$, they predicted $D/D_0 = 1.15$ and 1.08 at $\chi N = 25$ and 50, respectively, while we obtain 1.218 and 1.166, respectively. We note that our SCFT calculations are in good quantitative agreement with those of Cooke and Shi [7] obtained with the polydispersity expansion in equation (5).

The lower plot in Figure 3 shows the relative spacing, D/D_0, as a function of the composition, f, for a series of polydispersities, PDI_A, at the fixed segregation, $\chi N = 100$. (The reference spacing, $D_0 = 2.3367aN^{1/2}$, is still that of a symmetric monodisperse melt of equal segregation.) The main result of both the SCFT and SST predictions is that D increases monotonically with f. The second issue is the fact that the lamellar region shifts towards larger f as the polydispersity of the A block increases [7]. The precise location of the phase boundaries is beyond the scope of our present study, but nevertheless we have estimated them by equating the canonical free energies of the lamellar and cylindrical morphologies. Accurate boundaries would require that we equate the lamellar free energy to that of the gyroid phase, but that is too computational for our algorithm at this level of segregation. Furthermore, we should also account for the two-phase coexistence regions separating the pure lamellar and gyroid regions. In any case, the gyroid region [13] and the two-phase regions [7] are expected to be narrow, and so our estimated boundaries should be reasonably accurate.

We get a good idea of why the SST does so poorly for polydisperse melts by examining Figure 4 for the segment distributions of the different diblock molecular weights. Just as one would expect [7], the longer A blocks (*e.g.*, $\sigma = 3$) tend to occupy the center of the A domain, while the shorter ones (*e.g.*, $\sigma = 0.3$) tend to fill the space next to the interface. However, the very short A blocks (*e.g.*, $\sigma = 0.03$) are primarily in the middle of the B domain. Of course the explanation is simple; when the A block is so short, it is energetically favorable for it to enter the B domain thereby allowing the attached B block to relax. Indeed, Figure 4b shows that while most B blocks ($\sigma > 0.3$) are anchored to the interface as assumed by SST, the ones attached to small A blocks (*e.g.*, $\sigma = 0.03$) have been pulled away from the interface and are concentrated in the center of the B domain.

Figure 5 illustrates the degree to which the A blocks are dislodged from their domain as a function of their relative molecular weight, σ. The quantity plotted on the vertical axis is the integral of $\phi_A(z;\sigma)$ over one B domain divided by the overall period, D. (The B domain is defined

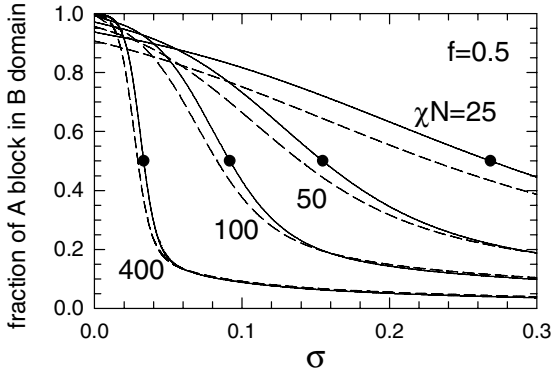

Fig. 5. Fraction of $\phi_A(z;\sigma)$ in the B domain plotted as a function of the A-block size, σ. The solid and dashed curves are calculated for $\mathrm{PDI}_A = 2$ and 1, respectively.

as the range of z over which $\phi_B(z) > 0.5$.) The solid curves are calculated for a polydispersity of $\mathrm{PDI}_A = 2$, but we also include dashed curves for the limit $\mathrm{PDI}_A \to 1$, illustrating that the actual value of PDI_A has a minimal effect on the results. Even though the curves remain nearly the same, a lower PDI_A still implies that there is a smaller population of short A blocks that get pulled into the B domain.

The solid dots in Figure 5 define a critical molecular weight, σ_{cr}, below which an A block has on average more segments in the B-rich domain than in the A-rich domain. This quantity is plotted in Figure 6 as a function of segregation and composition. The trends are best understood by appealing to the SST described in the appendix. The σ_{cr} at which the A blocks are *pulled out* of their domain by the B block can be estimated by equating the enthalpic cost of placing a short A block in the B domain to the reduction in free energy that occurs as one junction is removed from the A/B interface and the stretching energy of the B block is relieved. This condition is expressed as

$$\chi N f \sigma_{cr} = \frac{2aN^{1/2}}{D}\sqrt{\frac{\chi N}{6}} + \frac{\pi^2(1-f)D^2}{32a^2N}. \qquad (27)$$

Note that the entropic stretching energy of the A block is ignored, because it is assumed to be negligible relative to that of the B block (*i.e.*, $\sigma_{cr} \ll 1$). The resulting SST prediction is denoted in Figure 6 by dashed curves, and the agreement with SCFT is rather good. The SST certainly captures the behavior predicted by SCFT. It now becomes evident that PDI_A only impacts σ_{cr} through its small indirect effect on D, consistent with the difference in the solid and dashed curves in Figure 5.

So far, we have restricted our attention to molecules with only one polydisperse block (specifically, A). In principle, the SCFT is easily extended to two polydisperse blocks; equations (1) and (2) are simply generalized to

$$\phi_\alpha(\mathbf{r}) = \int_0^\infty \mathrm{d}\sigma_A \int_0^\infty \mathrm{d}\sigma_B p(\sigma_A,\sigma_B)\phi_\alpha(\mathbf{r};\sigma_A,\sigma_B), \quad (28)$$

$$\ln \mathcal{Q} \to \int_0^\infty \mathrm{d}\sigma_A \int_0^\infty \mathrm{d}\sigma_B p(\sigma_A,\sigma_B) \ln \mathcal{Q}(\sigma_A,\sigma_B), \quad (29)$$

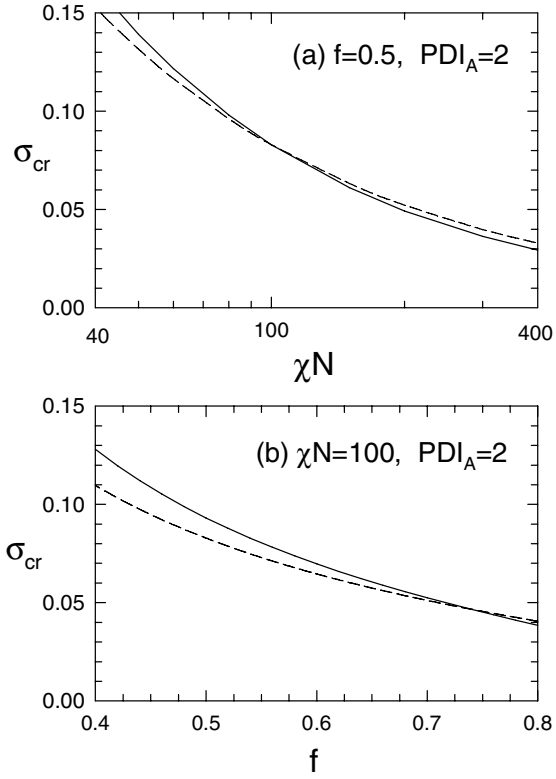

Fig. 6. Critical molecular weight, σ_{cr}, below which A blocks are pulled into the B domain plotted as a function of (a) segregation χN and (b) composition f. The solid curves denote the SCFT criterion represented by solid dots in Figure 5 and the dashed curves show the SST prediction from equation (27).

where $p(\sigma_A,\sigma_B)$ is the probability density of having a diblock with $fN\sigma_A$ A-type segments and $(1-f)N\sigma_B$ B-type segments. It is natural to assume that any synthesis would lead to a negligible correlation between the distribution of the two blocks [7], in which case

$$p(\sigma_A,\sigma_B) = p_A(\sigma_A)p_B(\sigma_B), \qquad (30)$$

where $p_A(\sigma_A)$ and $p_B(\sigma_B)$ would in general have distinct polydispersity indices, PDI_A and PDI_B, respectively. Note, however, that the form of equation (30) would not apply to the experiment of Matsushita *et al.* [4]. For those distributions to which it does apply, the spectral SCFT algorithm would proceed almost the same as before except for obvious generalizations to J_{ij} and K_i in equations (21) and (22) and to the free energy, F, in equation (26), where the single integrals are replaced by double integrals over σ_A and σ_B. Naturally, this implies a substantial increase in the computational cost, but our algorithm is so efficient that the calculation remains entirely feasible. This is illustrated by Figure 7, where the computational cost for two blocks of equal polydispersity (*i.e.*, $\mathrm{PDI}_A = \mathrm{PDI}_B$) is plotted relative to that of monodisperse molecules. Even for Gaussian quadratures of order $n_g \sim 100$, the CPU time only increases by a factor of ~ 6 as opposed to 10^4 as would be the case if all the molecular-weight combinations

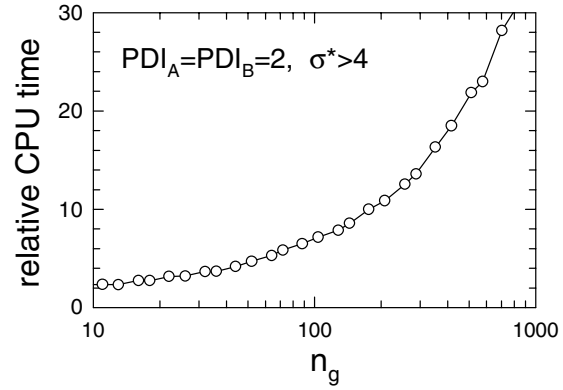

Fig. 7. Analogous plot to that of Figure 2a, but for the case where both blocks have identical degrees of polydispersity.

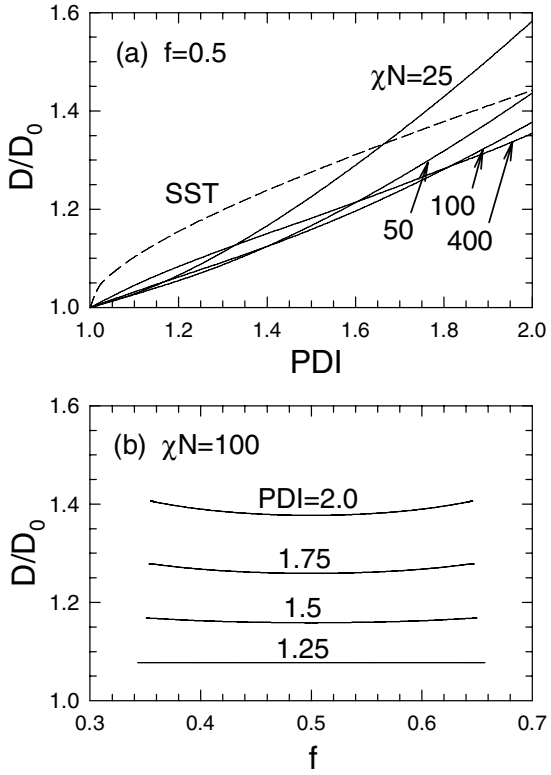

Fig. 8. Analogous plots to those of Figure 3, but for the case where both blocks have identical degrees of polydispersity, PDI $\equiv$ PDI$_A$ = PDI$_B$.

were calculated independently without the ground-state dominance approximation.

The effect of both blocks being polydisperse is demonstrated in Figure 8 by analogous plots to those in Figure 3. As before, the D spacing swells from that of the monodisperse melt, D_0, as the polydispersity increases, but now the effect is approximately doubled. However, the dependence on composition in Figure 8b is considerably different to that in Figure 3b. The fact that both blocks are equally polydisperse restores the $f \leftrightarrow (1-f)$ symmetry to the phase behavior. Consequently, the lamellar region remains centered around $f = 0.5$, and D ends up being relatively independent of f. Incidentally, the SST predicts that D is completely independent of f for PDI$_A$ = PDI$_B$, which is why we have not bothered to include it in Figure 8b.

4 Discussion

We have partially resolved the reported discrepancy [5] between theory and experiment regarding the inflated domain spacing produced by polydispersity. Our SCFT calculation now predicts that the induced swelling persists into the strong-segregation regime, which is further substantiated by SST. Still, the predicted level of swelling is significantly less than the measured values. At $\chi N = 100$, a polydispersity of PDI$_A$ = 2 in one of the blocks results in a predicted swelling of $D/D_0 = 1.14$, whereas the experiments of Lynd and Hillmyer measured a ratio of $D/D_0 = 1.28$. However, there are various possible explanations, in addition to the significant experimental uncertainties in measuring χN and PDI$_A$. For instance, the experimental estimate is based on a linear fit of D over the range PDI$_A$ = 1.42 to 1.94, which, according to the theory, would underestimate D_0 and thus overestimate the ratio D/D_0; granted however this could only explain a small portion of the discrepancy. A more significant factor might be the issue of how well the Schulz-Zimm distributions represent the experimental ones; more accurate distributions could be obtained by modeling the chemical synthesis. Another important issue is whether or not the lamellar samples are fully equilibriated at such high segregations as $\chi N \approx 100$; non-equilibrium effects can be sizable even at modest segregations of $\chi N \approx 40$ [14]. There is clearly a need for further experimental and theoretical investigation to understand the remaining discrepancy.

The inaccuracy in the previous SCFT calculation [5] can be attributed to the slow rate of convergence of the Gaussian-quadrature approximation (Eq. (4)) at large χN and PDI$_A$. This becomes evident only when the approximation is taken to extreme orders (*e.g.*, $n_g \to 10^3$) as illustrated by Figure 1a. We have investigated a number of other integration schemes, such as the Simpson method for $0 < \sigma < \sigma^*$ and analytical integration for $\sigma^* < \sigma < \infty$ made possible by the ground-state dominance approximation. The alternate schemes give consistent results, but are slightly less computationally efficient. Notably, however, they are more easily adapted to changes in the functional form of $p(\sigma)$.

The plots in Figures 2 and 7 testify to the efficiency of our spectral algorithm with respect to monodisperse melts. This still leaves the question of how computationally demanding are the monodisperse calculations, but that depends on the number of basis functions, M, required in equations (6) and (7), which in turn depends on the symmetry of the phase and the level of segregation. The CPU time required by the spectral calculation scales as approximately M^3 and the quasi–Newton-Raphson algorithm used to solve the self-consistent field equations and minimize the free energy with respect to D adds another factor of M, so that the overall time scales as roughly M^4. This implies that the method is exceptionally efficient

for small M, but is very costly for large M. Indeed, the monodisperse lamellar phase at $\chi N = 100$, only requires $M = 30$ basis functions and can be done in a mere 0.2 seconds on a modern desktop single-processor computer. However, the cylinder phase at the same segregation requires $M \approx 200$, which increases the computational time to about 10 minutes. The complex gyroid morphology, on the other hand, requires $M \approx 500$ just for an intermediate segregation of $\chi N = 40$, and this takes about 7 hours of CPU time. For such large values of M, it is better to replace the quasi–Newton-Raphson algorithm by alternative techniques such as Anderson mixing [15]. In any case, the additional factors of 2 to 6 for polydisperse melts are not generally a serious burden, and calculations remain manageable on single-processor machines.

Although the SST predictions for D/D_0 in Figures 3 and 8 are not particularly accurate, the SST does provide simple explanations for the SCFT trends. In all cases, the underlying reason for the behavior is that polydispersity reduces the entropic stretching energy, $F_{st,\alpha}$, by a factor S_α defined in equation (A.4). The reduction in stretching energy implies an increase in the relative size of the interfacial tension, γ_I, which then leads to larger domains. Naturally, the effect is greater when both domains (*i.e.*, $\alpha = A$ and B) are polydisperse. When there is an asymmetry in the level of polydispersity, the overall stretching energy is reduced by increasing the volume fraction of the more polydisperse domain, which explains why D/D_0 increases with f in Figure 3b and why D/D_0 is relatively independent of f in Figure 8b. The compositional shift in the lamellar region, indicated by Figure 3b, is also explained by the asymmetry in the stretching energies caused by unbalanced polydispersities. The explanation is the same as when a comformational asymmetry occurs between the A and B statistical segment lengths [16]; the boundaries shift because there is an advantage of curving the interface away from the domain with the higher stretching energy.

The quantitative inaccuracy of SST may be somewhat unexpected given how well it predicts the domain spacing of monodisperse melts [17]. The discrepancy with SCFT cannot be entirely attributed to the fact that SST ignores the *pull-out* of short blocks (*i.e.*, $\sigma < \sigma_{cr}$) from their domains, because the SST becomes inaccurate even for slight polydispersities, where there is still a negligible population of A blocks smaller than $fN\sigma_{cr}$. In reality, the previous success of SST in predicting the domain size is likely attributed to a fortuitous cancellation of finite-segregation corrections. One may suspect this by the fact that SST is generally inaccurate with respect to other quantities [18]. Indeed, detailed examination of finite-stretching corrections [19] does illustrate that a tremendous degree of chain stretching is required before the assumptions of SST are accurately realized.

Now that we have an efficient method of integrating over broad continuous molecular-weight distributions, the next challenge will be to extend the bulk phase diagrams of Cooke and Shi [7] to higher degrees of polydispersity. In that study, the phase boundaries were evaluated by equating the canonical free energies of the competing phases, but this ignores the emergence of two-phase coexistence regions. Their effect on binary diblock blends is well known; compare, for example, the diagrams in reference [20] where the two-phase regions are ignored to the diagrams in reference [21] where they are included. Certainly, Cooke and Shi have made a reasonable assumption that these regions are negligible for low degrees of polydispersity, but they will undoubtedly become significant for high polydispersities. The techniques for calculating two-phase regions are more involved for continuous molecular-weight distributions than for binary blends, but the methods have been well documented for macrophase separation in polydisperse polymer solutions [22]. Nevertheless, it still remains to be seen how easily the calculations for uniform phases are adapted to the structured phases of block copolymers.

5 Conclusions

We have introduced a new efficient SCFT algorithm for polydisperse block copolymers, which is demonstrated on diblocks with a fixed $(1 - f)N$ number of B-type segments and a distribution of $fN\sigma$ A-type segments specified by the probability density $p(\sigma)$. By using a spectral-based algorithm, the concentration profiles, $\phi_A(\mathbf{r};\sigma)$ and $\phi_B(\mathbf{r};\sigma)$, of additional molecular weights can be evaluated for a relatively minor computational expense. The efficiency is increased further by using the ground-state dominance approximation, whereby all molecular weights above $\sigma^* \approx 4$ can be evaluated without any additional cost. These strategies can be applied to a variety of integrations schemes, but the Gaussian quadrature suggested by Sides and Fredrickson [6] in equation (4) works well for the usual Schulz-Zimm distribution [10] specified by equation (3). Even for quadratures of order $n_g \sim 100$, the computational cost is only a couple times that of a monodisperse melt. In fact, the efficiency is sufficient that the algorithm can be readily extended to copolymers with two or more polydisperse blocks.

In this first instance, we have used our algorithm to resolve an apparent discrepancy, where the SCFT had failed to predict elevated domain spacings similar to those observed by experiments on strongly segregated melts [5]. The problem can be attributed to slow convergence of the Gaussian quadrature; by pushing the order, n_g, to much higher levels, the SCFT becomes consistent with experiment. We also show that strong-segregation theory (SST) predicts a similar increase in domain spacing, although the agreement with SCFT is not particularly good even at $\chi N = 400$. Some of the inaccuracy in SST can be attributed to the fact that it ignores the short A blocks (*i.e.*, $\sigma < \sigma_{cr}$) that are pulled from their domains by the strongly stretched B blocks. Although this *pull-out* effect is omitted by the conventional SST treatment, SST can still be used to estimate the critical molecular weight, σ_{cr}, below which the A blocks are dislodged. Our next goal will be to evaluate bulk phase diagrams similar to those of Cooke and Shi [7], but at higher degrees of polydispersity where two-phase regions are likely to become important.

We are grateful to Nate Lynd and Marc Hillmyer for useful discussions and to the EPSRC (EP/E010342/1) for funding this work.

Appendix A. Strong-segregation theory (SST)

When χN becomes large, the block-copolymer junction points localize in narrow interfacial regions while the A and B blocks segregate into strongly stretched polymeric brushes, transforming SCFT into the analytical strong-segregation theory (SST) of Semenov [23]. In this limit, the free energy can be separated as

$$F = \frac{2\mathcal{V}}{D}\gamma_I + F_{st,A} + F_{st,B}, \tag{A.1}$$

where

$$\gamma_I = k_B T a \rho_0 \sqrt{\frac{\chi}{6}} \tag{A.2}$$

is the interfacial tension between the A and B brushes and $\rho_0 = nN/\mathcal{V}$ is the overall segment density. The last two terms in equation (A.1) represent the entropic-energy cost of stretching the A and B blocks, respectively. Milner *et al.* [24] have worked out the general expression for a polydisperse brush as

$$\frac{F_{st,\alpha}}{nk_BT} = \frac{\pi^2 D_\alpha^2}{8a^2 N_\alpha} S_\alpha, \tag{A.3}$$

where D_α is the brush thickness and N_α is the number-averaged polymerization of the chains. (For the A brush, $D_A = fD/2$ and $N_A = fN$, and for the B brush, $D_B = (1-f)D/2$ and $N_B = (1-f)N$.) The effect of the polydispersity distribution, $p_\alpha(\sigma)$, on the stretching energy is contained entirely within the factor

$$S_\alpha \equiv \int_0^\infty \mathrm{d}\sigma \left[1 - \int_0^\sigma \mathrm{d}\sigma' p_\alpha(\sigma')\right]^3, \tag{A.4}$$

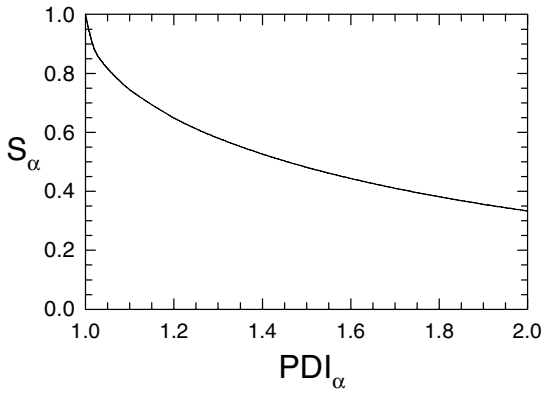

Fig. 9. Relative reduction in entropic stretching energy of a polymer brush (Eq. (A.4)) plotted as a function of the polydispersity index, assuming the Schulz-Zimm distribution (Eq. (3)).

which is plotted in Figure 9 for the Schulz-Zimm distribution. The fact that S_α is monotonically decreasing implies that polydispersity reduces the stretching energy, which ultimately results in larger domains. The actual equilibrium periodicity, obtained by minimizing F, works out to be

$$D = D_0 \left[fS_A + (1-f)S_B\right]^{-1/3}, \tag{A.5}$$

where

$$D_0 = 2\left(\frac{8\chi N}{3\pi^4}\right)^{1/6} aN^{1/2} \tag{A.6}$$

is the lamellar period for a monodisperse melt.

References

1. F.S. Bates, G.H. Fredrickson, Phys. Today **52**, 32 (1999); M.W. Matsen, J. Phys.: Condens. Matter **14**, R21 (1994).
2. D. Bendejacq, V. Ponsinet, M. Joanicot, Y.-L. Loo, R.A. Register, Macromolecules **35**, 6645 (2002).
3. A.-V. Ruzette, S. Tencé-Girault, L. Leibler, F. Chauvin, D. Bertin, O. Guerret, P. Gérard, Macromolecules **39**, 5796 (2006).
4. Y. Matsushita, A. Noro, M. Iinuma, J. Suszuki, H. Ohtani, A. Takano, Macromolecules **36**, 8074 (2003).
5. N.A. Lynd, M.A. Hillmyer, Macromolecules **38**, 8803 (2005).
6. S.W. Sides, G.H. Fredrickson, J. Chem. Phys. **121**, 4974 (2004).
7. D.M. Cooke, A.-C. Shi, Macromolecules **39**, 6661 (2006).
8. L. Leibler, H. Benoit, Polymer **22**, 195 (1981); K.M. Hong, J. Noolandi, Polym. Commun. **25**, 265 (1984); C. Burger, W. Ruland, A.N. Semenov, Macromolecules **23**, 3339 (1990); **24**, 816 (1991).
9. M.W. Matsen, M. Schick, Phys. Rev. Lett. **72**, 2660 (1994).
10. G.V.Z. Schulz, Z. Phys. Chem. (Munich) **B43**, 25 (1939); B.H. Zimm, J. Chem. Phys. **16**, 1099 (1948).
11. G. Arfkin, *Mathematical Methods for Physicists* (Academic Press, San Diego, 1995).
12. M.W. Matsen, in *Soft Matter*, Vol. **1**: *Polymer Melts and Mixtures*, edited by G. Gompper, M. Schick (Wiley-VCH, Weinheim, 2006).
13. E.W. Cochran, C.J. Garcia-Cervera, G.H. Fredrickson, Macromolecules **39**, 2449 (2006); 4264 (2006).
14. P.M. Lipic, F.S. Bates, M.W. Matsen, J. Polym. Sci., Part B **37**, 2229 (1999).
15. R.B. Thompson, K.O. Rasmussen, T. Lookman, J. Chem. Phys. **120**, 31 (2004).
16. M.W. Matsen, F.S. Bates, J. Polym. Sci., Part B **35**,945 (1997).
17. M.W. Matsen, F.S. Bates, Macromolecules **29**, 1091 (1996).
18. M.W. Matsen, F.S. Bates, J. Chem. Phys. **106**, 2436 (1997).
19. M.W. Matsen, J. Chem. Phys. **121**, 1938 (2004).
20. A.-C. Shi, J. Noolandi, Macromolecules **28**, 3103 (1995).
21. M.W. Matsen, F.S. Bates, Macromolecules **28**, 7298 (1995).
22. P. Sollich, J. Phys.: Condens. Matter **14**, R79 (2002).
23. A.N. Semenov, Sov. Phys. JETP **61**, 733 (1985).
24. S.T. Milner, T.A. Witten, M.E. Cates, Macromolecules **22**, 853 (1989).